Deducing Erosion Rates of the Mt. Langley Summit Flat using ^{21}Ne in Quartz

Curtis Baden[1]

David L. Shuster[1,2] **, Advisor**

Greg Balco[2]**, Collaborator**

1: Earth and Planetary Science; University of California, Berkeley

2: Berkeley Geochronology Center

A thesis submitted in partial fulfillment

of the requirements for the

Degree of Bachelor of Arts with Honors

in Geology

University of California, Berkeley

Berkeley, California

June 17, 2013

Abstract:

We investigated the effective erosion rate acting on the high alpine summit flat surfaces in the southern Sierra Nevada using measurements of cosmogenic ^{21}Ne in quartz. Samples were taken from the Mt. Langley summit, at elevations around 4250 m. Using observed molar concentrations of ^{21}Ne, we estimate an average erosion rate of 9.5 ± 0.5 m/Myr across the summit sample set, with erosion rates ranging from 6.8 – 14.6 m/Myr. We collected three distinct sample types from the summit surface: loose rock, summit boulder, and bedrock tor samples. While we infer small differences in erosion rate between sample types, the small data set limits the degree to which these differences can be interpreted. All samples, with the exception of two summit boulder samples, measured within one standard deviation of the average erosion rate for the summit flat. Summit boulder samples exhibited greater variability in erosion rate, representing the highest, lowest, and medial rates measured across the sample set. We attribute this variation to complicated and variable exposure history among the boulders sampled. This variability may yield insight into the processes by which these boulders form, erode, and reorient themselves amidst an environment which is over long timescales steadily eroding and lowering at a rate of 9.5 m/Myr.

1) Introduction:

Summit flats, starkly distinguishable in the high altitude, mountainous landscapes in which they are found, have served as a source of curiosity and a platform for geomorphological study for over a century, with more quantitative analyses conducted on these peculiar features in the past twenty years (Munroe, 2005). These features, as defined by Small and Anderson (1998), exhibit gentle slopes of less than 0.3 m/m (16.7 degrees), and form at elevations above 3400 meters within the mid-latitude mountain ranges of the United States, among other global localities. While high altitude landscapes may be littered with locally flat terrain, true summit flats are defined as areas with a surface area greater than 5×10^{-2} km^2. Based on the observations of Small and Anderson (1998), summit flats have never been inundated by glacial ice of significant depth. Glacial polish, striations, chatter marks, and glacial erratics are absent in such areas. Regolith and bedrock-deduced debris predominantly comprise summit flat surfaces; the evacuation of such surface debris, as is expected in glacially scoured landscapes, is not observed. Given the absence of glacial relics, Anderson (2002) hypothesizes that summit flats have been formed in-situ under periglacial climate conditions. Prime targets for exposure age and erosion rate studies, summit flat surfaces have hosted a series of cosmogenic radionuclide measurements. Small et al. (1997) sampled summit flats in four ranges in the western United States, including the Beartooth, Wind River, Sierra

Nevada, and Front Ranges. Using Be^{10} and Al^{26}, Small et al. (1997) found the effective mean bedrock lowering rate of these ranges to be 7.6 ± 3.9 m / My.

^{21}Ne, a rare, cosmogenic stable isotope of neon, is commonly used to determine exposure ages, erosion rates, and sediment production and transport rates (Dunai, 2010). Produced in quartz alongside other cosmogenic nuclides (^{10}Be, ^{26}Al), ^{21}Ne forms largely by neutron spallation following cosmic ray bombardment of surface material. In measuring ^{21}Ne in quartz, the dominant spallation reaction of interest is $^{28}Si(n,2\alpha)^{21}Ne$. ^{21}Ne is a stable nuclide, and thus accumulates linearly with production for a non-eroding surface, unlike ^{10}Be and ^{26}Al. However, the molar concentration of a cosmogenic nuclide (i.e., moles of nuclide per mass of mineral) is a function of at least variables: exposure age and erosion rate. For an estimated production rate, therefore, ^{21}Ne concentration of a given sample yields a minimum exposure age. In environments experiencing long term steady state erosion, such as the summit flat surfaces described above, ^{21}Ne concentrations are no longer dependent on exposure age, but rather on regional erosion rates (Dunai, 2010). While particular value of ^{21}Ne measurements typically arises from analyzing very old surfaces (>5 My) and slowly eroding surfaces (<10cm/My), we apply these measurements to younger, relatively rapidly eroding surfaces evident in summit flat conditions.

The California southern Sierra Nevada exhibit high elevation landscapes which meet the criteria for summit flats as outlined by Small and Anderson (1998). The Mt. Langley summit and the surrounding terrain indeed meet these qualifications. Small et al. (1997) sampled summit flat erosion rates within the Sierra Nevada at a different location, though these rates were deduced from ^{10}Be and ^{26}Al measurements. ^{21}Ne measurements from samples within the Sierra Nevada have been seldom conducted due to relatively low production rates at the latitudes of interest. We collected six samples on the summit of Mt. Langley using various sampling strategies in order to analyze and quantify erosion rates acting on the high altitude southern Sierra Nevada using ^{21}Ne. At an elevation of 4,275 meters with minimal topographic shielding, the Mt. Langley summit flats are ideal for ^{21}Ne analysis given the relatively high production rate of ^{21}Ne for the site latitude.

2) Methods

In order to simplify exposure correction during analysis, each sample was collected from a relatively flat area, with no significant changes in local topography within 2-3 meters of the sample collection site. We collected samples that were minimally shielded from the horizon in all directions. We measured macroscopic, topography-induced horizon disruptions for each sample with a brunton compass by hand, and recorded these disruptions for shielding corrections in the analysis stage of the study. Rock surfaces from which samples were specifically taken were flat, local high points to ensure minimal exposure disruption. Due to equipment weight limitations, sample collection was limited to specific locations

(meeting the above criteria) where thin nodules of boulders and bedrock tors could be broken off of the larger rock masses using a standard sized rock hammer.

We collected six samples from the debris-laden summit (Fig. 2) and two samples from the recently glacially scoured bedrock surface of a nearby cirque floor. This sampling strategy allowed for comparison of ^{21}Ne concentrations between non-glaciated summit surfaces and the fairly recently glaciated cirque samples in common lithology. We invoked a separate strategy for summit sampling. The six summit samples collected fall into three classifications: Loose rock samples, summit boulder-derived samples, and bedrock tor derived samples. As all samples are ultimately derived from the same granitic rock type, we intended to explore differences in exposure age and erosional history between the bedrock, boulder, and loose rock samples in the summit flat environment. We noted and recorded the orientation of each sample relative to the sky and to the rock mass from which the sample was removed, and photographed and recorded the GPS-derived location of all sample sites. Sample and site data are summarized in Table 1. GPS recorded locations for all samples are depicted in Figure 1. Sample weight and receding daylight atop the Mt. Langley summit limited the summit sample size to the six samples collected.

Following the collection trek, we photographed each sample and recorded the dimensions for thickness corrections to be made after ^{21}Ne concentration measurements. We then crushed all samples to a 2 mm grain size, and hand-picked quartz grains from the crushed rock mass. The collected quartz was fairly pure and lacked significant visible inclusions, and thus was not etched in HF prior to analysis. We measured the isotopic composition of Ne (i.e., the molar abundances of ^{20}Ne, ^{21}Ne, and ^{22}Ne) within the isolated quartz grains for each sample in the Noble Gas Thermochronometry Lab at Berkeley Geochronology Center. The quartz was heated to a controlled temperature using a 150 W diode laser and a pyrometer feedback loop. After heating, the extracted gas was purified and passed into a sector field noble gas mass spectrometer. The samples were analyzed using a three stage stepwise heating process (400°C, 850°C, 1100°C); we then plot the observed ratios on three-isotope plots (i.e., ^{22}Ne/^{20}Ne versus ^{21}Ne/^{20}Ne). We then calculate total ^{21}Ne concentrations (prior to nucleogenic corrections) from these data by deconvolving atmospheric Ne by assuming the observed gas is a mixture between atmospheric and cosmogenic Ne (Niedermann et al., 1994).

To estimate the site-specific production rate of ^{21}Ne, we first calculated the ^{10}Be production rate for each sample using the Balco et al. (2009) North-eastern North America (NENA) ^{10}Be production rate and the Stone (2000) scaling scheme given the sample locations and elevations. We then scaled these values to the production rate for ^{21}Ne using the ^{21}Ne/^{10}Be production ratio of 4.08 reported by Balco and Shuster (2009). We accounted for topographic shielding and sample thickness corrections using the methodology outlined by Balco et al. (2008) in calculating individual sample production rates. Table 2 summarizes the ^{21}Ne production rate derivation methodology we assume for this study. We then calculated apparent

exposure ages based on the ^{21}Ne concentrations and production rates of the samples, and deduced erosion rates from these ages.

3) Results

Our results are summarized in Table 3. We observed a significant difference in ^{21}Ne concentrations between the summit and cirque floor samples, as was expected given the evidence of glaciation within the cirque basin. Summit samples on average exhibited 18.75 ± 0.45 Matoms ^{21}Ne /g, as compared to the cirque floor sample average of 7.22 ± 0.91 Matoms ^{21}Ne/g. Production rates calculated for the summit and cirque floor sites differ significantly as a result of variable topographic shielding between the sites and the effect of elevation on ^{21}Ne production. The average production rate for summit samples is 239.0 atoms ^{21}Ne/g/year, and the production rate for the cirque floor samples is 137.4 atoms ^{21}Ne/g/year.

The three isotope plot (Fig. 3) for the summit samples shows that the data fall along the spallation-induced Ne ratio line, indicating that the ^{21}Ne in the summit samples was largely produced by interaction with cosmic radiation. However, these points plot sufficiently low along this spallation line that they are also indistinguishable from the nucleogenic composition line (Niedermann et al., 1994). Note that many of the data points in the cirque valley floor three isotope plot lie below the spallation line, and closer to the nucleogenic line. While the ^{21}Ne we observed in quartz is largely produced cosmogenically, we assume that these samples may also contain nucleogenic ^{21}Ne. Nucleogenic ^{21}Ne within the bulk sample rock, primarily resulting from the reactions $^{18}O(\alpha,n)^{21}Ne$ and $^{24}Mg(n,\alpha)^{21}Ne$, is produced in Uranium and Thorium baring minerals as a result of α particle production due to radioactive decay (Wetherill, 1954). In granitic lithologies, Uranium and Thorium primarily reside in the accessory minerals monazite, zircon, and apatite (Bea, 1996). As quartz contains minimal amounts of the elements Uranium and Thorium, nucleogenic ^{21}Ne is not produced in significant quantities within quartz itself. However, minerals rich in these elements may implant α particles within the outer portions of neighboring quartz grains as Uranium and Thorium decay (Amidon et al., 2009). Quartz grains neighboring such minerals are therefore subject to the production of nucleogenic ^{21}Ne along their grain boundaries alongside the cosmogenically produced ^{21}Ne within the entire mineral grain. As the cosmogenic ^{21}Ne concentrations of these samples are not high enough to exclude the presence of nucleogenic ^{21}Ne (as is suggested by the three isotope plot), it is important to quantify the abundance of nucleogenic ^{21}Ne that may also be present in these samples.

We employed the following procedure as a means of correcting for the nucleogenic ^{21}Ne content within these samples. Assuming that glacial ice was last present in the cirque basin 13,000 years ago, and given the averaged cirque floor ^{21}Ne concentration (7.22 Matoms/g) and production rate (137.4

atoms/g/yr), we deduced the maximum post-glacial cosmogenic ^{21}Ne accumulation within these samples. We assume no interruptions in exposure, and we assume that glaciation of the cirque floor removed all cosmogenic isotopes prior to re-exposure 13000 years ago. Of the measured 7.22 Matoms/g, the above reasoning suggests that only 1.79 Matoms/g were produced cosmogenically. Therefore, based on this calculation and its assumptions, the minimum nucleogenic ^{21}Ne present in the Mt. Langley sample set is assumed to be 5.43 Matoms ^{21}Ne/g. The cosmogenic and nucleogenic ^{21}Ne concentrations we calculate in the above procedure are consistent with those obtained through more complex analyses conducted by Niedermann et al. (1994), who also focus on Ne isotopes in quartz derived from Sierra Nevada granites within cirque basins. Correcting for the nucleogenic Ne, the average cosmogenically produced ^{21}Ne concentration for summit samples is 13.32 ± 1.01 Matoms ^{21}Ne/g.

Accounting for nucleogenic Ne, calculations of apparent exposure ages for summit samples yield an average value of 53,900 ± 3,700 years. Because ^{21}Ne is stable it is only removed from exposed surface material by erosional processes. Therefore, this apparent exposure age represents the time scale over which rock on the Mt. Langley summit is eroded away following initial exposure to cosmic ray bombardment and thus initial ^{21}Ne production, following the reasoning outlined by Dunai (2010). Based on these apparent exposure ages, we calculated erosion rates for each of the Langley summit samples. These erosion rates range from 6.8 ± 1.0 to 14.6 ± 4.3 m/Myr, with a weighted average value of 9.5 ± 0.5 m/Myr. Loose rock, summit boulder, and bedrock tor samples exhibited small observable differences in erosion rate, though the small sample size for each classification limits the extent to which these results can be interpreted. Summit boulders exhibited the highest degree of variability, as the highest and lowest erosion rates observed for the sample set were measured from these boulder-deduced samples. Summit boulders, however, were represented by the largest number of samples (3 samples), as compared to bedrock tors (2 samples) and loose summit rock samples (1 sample).

4) Discussion

The summit flats sampled in this study exhibit the characteristics generally observed for these terrains. The Langley summit and the surrounding topography is gently sloping, is absent of evidence of previous glacial occupation (striations, chatter marks, glacial polish) and occupies an area greater than 5×10^{-2} km^2. The summit is also inundated with large boulders and debris, which would be absent if the surface had indeed been glaciated. While early models of cold-based glaciers entertained the idea that such glaciers would not entrain bed material into basal layers of flowing glacial ice (and hence Mt. Langley's debris-laden summit could have been glaciated without debris evacuation), Cuffey (2000) suggests otherwise. Interpolating from these findings, any prior glacial occupation of summit flats would

result in at least minimal debris evacuation and bed scour. Langley's summit shows no observable evidence of this kind.

The lowering of summit flat surfaces is purely driven by periglacial creep of unconsolidated material due to the absence of observed landsliding, fluvial activity, and glacial scour atop these surfaces (Small et al., 1997). The bedrock lowering rates sampled by Small et al. effectively yield a proxy for the lowering rate of these summit surfaces as a whole. The average erosion rate of 9.5 ± 0.5 m/Myr calculated above represents the lowering rate of the Mt. Langley summit in particular, which was not specifically sampled by Small et al. (1997). However, this value is consistent with Small's calculated average of 7.6 ± 3.9 m/Myr. CRN-driven measurements reported by Small and Anderson (1998) of erosion in nearby basins and glacial troughs report erosion rates an order of magnitude higher than rates observed for summit flats. When these valleys and troughs are occupied by glacial ice, summit flat erosion (on the order of 5-15 micrometers/yr) is two to three orders of magnitude slower than erosion rates within glacial troughs as a result of glacial scour (~1mm/yr). As we used the cirque floor sample data to estimate nucleogenic ^{21}Ne concentrations within the sample set, we do not report erosion rates for the cirque floor samples in this study. However, given the difference in erosion rates measured by Small and Anderson (1998), ranges containing summit flats are thus generally characterized by high relief, as summits erode at a much slower rate than the surrounding terrain. In the Laramide ranges in the western United States, the onset of relief production is predicted to have begun roughly three million years ago, and was likely associated with alpine glaciation (Small and Anderson, 1998). It is likely that glacial troughs seen today originated from the accumulation of snow and ice in paleo-fluvial channels prior to major relief production (Anderson, 2002). We suggest a similar relief production history for the High Sierra terrain in this study, despite not having specifically measured the erosion rates of the cirque samples.

Small et al. (1997) measured erosion rates of Lamarck Peak in the Sierra Nevada, deducing average erosion rate values of 3.1 ± 1.6 m/Myr and 2.9 ± 1.4 m/Myr from ^{10}Be and ^{26}Al measurements, respectively. While Lamarck Peak and Mt. Langley are separated by hundreds of miles, we make the comparison between the two sites because both sites dwell within the Sierra Nevada at very high elevation, and thus are likely subject to similar environmental and exposure conditions. The average erosion rate measured in this study, 9.5 ± 0.5 m/Myr, is well above that measured for the Lamarck Peak samples. This difference can likely be attributed to the variability in sampling strategies between the two studies, however. Small et al. (1997) collected samples specifically from broad, smooth, flat tops of bedrock tors and the largest boulders present on the summit flat regions of interest. While select samples of the Mt. Langley set met these selection criteria, we did not go to great lengths to ensure that each sample met these requirements. We chose a sampling strategy in hopes of measuring the differences

between exposure ages and erosion rates among the various sample types (loose rock, bedrock tor, and summit boulders) discussed above.

Measurements for all samples, with the exception of L2 SUM (a summit boulder sample), are within one standard deviation of one another. Despite the lack of a strong distinguishable difference between the various summit sample types (in part due to the small sample size) these erosion rates together represent an average erosion rate for the Langley summit as a whole across a variety of surfaces. The loose rock sample (L1 SUM), with an erosion rate of 12.8 ± 3.1 m/Myr, suggests slightly more rapid erosion than most other summit samples. As a loose rock sample, the exposure history of this specimen is unknown, and potentially more complex than that which we assume for these measurements. Small et al. (1997) argue that summit flats erode in incremental, finite steps as chips (~10 cm) are removed from bedrock and summit boulders. The loose rock sample collected may represent such a chip, though one might expect an aged and weathered chip sample to exhibit a higher apparent exposure age and a lower erosion rate than is measured for the summit flat as a whole. This sample records a faster erosion rate than was calculated for the Mt. Langley summit flat, however. The specimen's small size may contribute to a faster observed erosion rate. As a specimen decreases in dimension due to erosion, the surface area to volume ratio increases, and thus smaller samples will likely erode faster than larger samples as a greater relative percentage of surface area is subject to erosional processes. By this logic, a small loose rock will thus erode faster than a large, voluminous boulder. This effect may not be able to account for the difference in erosion rate we observe for this sample, however, given the insignificance of chemical denudation in these high alpine environments. Considering the fact that all samples were sufficiently thin and nodular enough to be removed from the parent rock material with a standard rock hammer, all samples may also be affected by this artificial erosion rate enhancement, if it is indeed applicable. It is important to note that this measurement, while higher than most others, is still within one standard deviation of other measurements.

^{21}Ne concentrations from both bedrock tor samples (L4 SUM, L5 SUM) suggest a bedrock erosion rate of 11.3 m/Myr, with standard deviations of 1.7 m/Myr and 1.5 m/Myr, respectively. Despite the small sample size, the consistency between the two samples adds confidence to this measurement. Bedrock tors likely experience the least complex exposure histories of the sample types collected, in that they cannot be reoriented by settling debris. Surfaces exposed to cosmic ray bombardment remain exposed until they are eroded away in the chipping dominated mechanism suggested by Small et al. (1997), or become boulders themselves as the tors erode away along fractures and joint planes and separate from crystalline bedrock. While boulder shielding of bedrock could complicate exposure histories, we selected bedrock sites that were absent of boulders and similar debris.

Summit boulder erosion rates are highly variable, as they represent the highest, lowest, and median values for the sample set. L2 SUM, one of two summit samples from which an erosion rate was calculated that is *not* within one standard deviation of the sample average, was collected from a summit boulder, and exhibits an erosion rate of 6.8 ± 1.0 m/Myr, nearly half that of other samples. L3 SUM, also collected from a summit boulder, exhibits the highest erosion rate of the sample set (14.6 ± 4.3 m/Myr), and also lies outside one standard deviation from the 9.5 ± 0.5 m/Myr average. The high variability in summit boulder erosion rates observed is interesting, in that it might suggest that boulder-laden landscapes of the high alpine summit flats (exemplified in Fig. 2) evolve non-uniformly with respect to boulder production and subsequent boulder erosion. As these high alpine surfaces steadily erode, the boulders may topple and change orientation as they settle amongst the eroding debris, exposing new surfaces to cosmic ray bombardment and erosional processes and complicating their exposure history. Toppling and tumbling summit boulders would also likely increase the net erosion rate of summit flats as a whole if boulders were to mechanically crack and cleave as they reoriented. As current landscape models of these summit flats attribute virtually all sediment production and down-slope transport to frost creep and solifluction (Anderson, 2002), the mechanical breaking of boulders could measurably contribute to the net down-slope movement of material. Future studies involving the collection of many samples for each sample type using strict selection criteria might resolve the differences in erosion rate between sample types more clearly. Resolving these differences, if they indeed exist, would prove valuable in establishing a more data-supported erosional model for boulder reorientation and more broadly for summit flat surfaces.

5) Conclusion

This study quantifies the erosion rate of the Mt. Langley summit flat using ^{21}Ne in quartz. With the exception of Niedermann et al. (1994), there is very little, if any, published work conducted within the Sierra Nevada which focuses on Ne isotope applications. We collected eight total samples for analysis, six of which were collected from the summit and specifically used to calculate erosion rates for the high alpine surface. The remaining two cirque floor samples contained significantly less ^{21}Ne than the summit samples, and for the purpose of this study were used to calculate the amount of nucleogenic ^{21}Ne inherent in the rock body. This value was then subtracted from each of the summit sample's total ^{21}Ne concentration to estimate the cosmogenic ^{21}Ne concentration. We intend to improve the nucleogenic ^{21}Ne concentration estimation made in this study by measuring Uranium concentrations in quartz grains within each of the samples. This will constrain the "nucleogenic" ^{21}Ne abundance that is specific to each sample, thus more accurately quantifying the cosmogenic ^{21}Ne for each of the eight samples. Based on our current estimates, however, erosion rates averaged across the six summit samples yield an approximate value of

9.5 m/Myr for the Mt. Langley summit flat. This value is significantly higher than the erosion rate calculated by Small et al. (1997) for Lamarck Peak, another summit flat surface within the Sierra Nevada. The difference between these studies may be attributed to differences in sample collection strategy, however. With regard to the sample strategy employed for this study, we observed only slight differences in erosion rates between the three sample types collected (loose rock, summit boulder, bedrock tor), which may prove to be insignificant given the small sample sizes of each type. Summit boulders exhibited a large degree of variability in measured erosion rates, which may reflect complex erosion and exposure histories associated with boulder formation, weathering, and subsequent reorientation of regolith. Future studies focused on collecting additional samples from loose rock material, summit boulders, and bedrock tors may be able to more supportably discern existing differences in exposure ages and erosion rates of these surfaces.

References:

Amidon, W.H., Rood, D.H., Farley, K.A., 2009. Cosmogenic ^{3}He and ^{21}Ne production rates calibrated against ^{10}Be in minerals from the Coso volcanic field. *Earth and Planetary Science Letters* 280: 194-204.

Anderson, R.S., 2002. Modeling the tor-dotted crests, bedrock edges, and parabolic profiles of high alpine surfaces of the Wind River Range, Wyoming. *Geomorphology* 46: 35-58.

Balco, G., Stone, J., Lifton, N., Dunai, T., 2008. A complete and easily accessible means of calculating surface exposure ages or erosion rates from ^{10}Be and ^{26}Al measurements. *Quaternary Geochronology* 3: 174–195.

Balco G., Briner J., Finkel R.C., 2009. Regional beryllium-10 production rate calibration for late-glacial northeastern North America. *Quaternary Geochronology* 4: 93–107.

Balco, G., Shuster, D.L., 2009. Production rate of cosmogenic 21Ne in quartz estimated from 10Be, 26Al, and 21Ne concentrations in slowly eroding Antarctic bedrock surfaces. *Earth and Planetary Science Letters* 281: 48-58.

Bea, F., 1996. Residence of REE, Y, Th and U in Granites and Crustal Protoliths; Implications for the chemistry of crustal melts. *Journal of Petroleum Science and Engineering* 37(3): 521-552.

Cuffey, K.M., Conway, H., Gades, A.M., Hallet, B., Lorrain, R., Severinghaus, J.P., Steig, E.J., Vaughn, B., White, J.W.C., 2010. Entrainment at Cold Glacier Beds. *Geology* 28: 351-54.

Dunai, Tibor J. (2010) *Cosmogenic Nuclides: Principles, Concepts and Applications in the Earth Surface Sciences.* Cambridge, MA: Cambridge University Press.

Munroe, Jeffery S., 2005. Investigating the spatial distribution of summit flats in the Uinta Mountains of northeastern Utah, USA. *Geomorphology* 75: 437-49.

Niedermann, S., Graf, T., Kim, J., Kohl, C., Marti, K., Nishiizumi, K., 1994. Cosmic-rayproduced neon in terrestrial quartz: the neon inventory of Sierra Nevada quartz separates. *Earth and Planetary Science Letters* 125: 341–355.

Small, E.E., Anderson, R.S., Repka, J.L., Finkel, R., 1997. Erosion rates of alpine bedrock summit surfaces deduced from in situ “Be and 26A1. *Earth and Planetary Science Letters* 150: 413-25.

Small, Eric E., and Robert S. Anderson, 1998. Pleistocene Relief Production in Laramide Mountain Ranges, Western United States. *Geology* 26: 23-26.

Stone, J.O., 2000. Air pressure and cosmogenic isotope production. *Geophysical Research Letters* 105 (B10): 23753–23759.

Wetherill, G.W., 1954. Variations in the isotopic abundances of neon and argon extracted from radioactive minerals. *Physical Review* 96: 679-683.

Tables and Figures

Sample name	Latitude	Longitude	Elevation (m)	Thickness (cm)	Density	Shielding
L1 SUM	36.5233	-118.2398	4275	4	2.65	0.9999
L2 SUM	36.5232	-118.2398	4275	4	2.65	0.9999
L3 SUM	36.5229	-118.2397	4272	5	2.65	0.9999
L4 SUM	36.5229	-118.2384	4270	10	2.65	0.9999
L5 SUM	36.5228	-118.2383	4270	12	2.65	0.9999
L6 SUM	36.5225	-118.2380	4265	4	2.65	0.9999
CVF1	36.4977	-118.2356	3414	6	2.65	0.895
CVF2	36.4977	-118.2357	3414	5	2.65	0.895

Table 1: Sample Site Data. We collected latitude and longitude coordinates using a hand-held GPS device during sample collection. We recorded elevation values for each site using a 1:31680 topographic map. We measured the inclination of features on the horizon which constituted significant topographic shielding with a brunton compass and recorded for each sample, from which total topographic shielding was later calculated.

Sample name	Thickness correction	Estimated ^{10}Be production rate			^{21}Ne/^{10}Be production ratio	Estimated ^{21}Ne production rate
		(muons)	(spallation)	(total)	(Balco and Shuster, 2009)	(atoms/g/yr)
L1 SUM	0.9676	0.646	59.23	59.876	4.08	244.29408
L2 SUM	0.9676	0.646	59.23	59.876	4.08	244.29408
L3 SUM	0.9597	0.642	58.66	59.302	4.08	241.95216
L4 SUM	0.9216	0.629	56.27	56.899	4.08	232.14792
L5 SUM	0.9069	0.624	55.37	55.994	4.08	228.45552
L6 SUM	0.9676	0.644	58.93	59.574	4.08	243.06192
CVF1	0.9519	0.511	33.04	33.551	4.08	136.88808
CVF2	0.9597	0.513	33.31	33.823	4.08	137.99784

Table 2: ^{21}Ne Production Table. All reported values account for sample thickness and for topographic shielding, as is reported for each sample in the site data sheet. We obtained all production rates using the Stone (2000) scaling scheme and the NENA ^{10}Be production rate reported by Balco et al. (2009). We deduced ^{21}Ne production rates from these values using the ^{21}Ne/^{10}Be production ratio reported by Balco and Shuster (2009).

Sample Name	Sample Source (Type)	^{21}Ne - Initial Measured Values (Matoms/g)	^{21}Ne - Corrected Cosmogenic (Matoms/g)	Production Rate (^{21}Ne) (atoms/g/yr)	Apparent exposure age (ky)	Apparent erosion rate (m/Myr)
L1 SUM *	Loose Rock	16.87 ± 1.97	11.44 ± 2.79	244.3	46.8 ± 11.4	12.8 ± 3.1
L2 SUM*	Summit Boulder	27.06 ± 3.10	21.62 ± 3.23	244.3	88.5 ± 13.2	6.8 ± 1.0
L3 SUM	Summit Boulder	15.34 ± 2.79	9.91 ± 2.93	242.0	40.9 ± 12.1	14.6 ± 4.3
L4 SUM	Bedrock Torr	17.78 ± 1.57	12.35 ± 1.81	232.1	53.2 ± 7.8	11.3 ± 1.7
L5 SUM	Bedrock Torr	17.55 ± 1.32	12.12 ± 1.60	228.5	53.0 ± 7.0	11.3 ± 1.5
L6 SUM	Summit Boulder	18.08 ± 1.83	12.65 ± 2.04	243.1	52.0 ± 8.4	11.5 ± 1.9
SUM Mean		18.75 ± 0.45	13.32 ± 1.01	239.0	53.9 ± 3.7	9.5 ± 0.5
CVF 1 *	Cirque Floor	7.15 ± 1.13	1.72 ± 1.45	136.9		
CVF 2 †	Cirque Floor	7.41 ± 1.73	1.98 ± 1.95	138.0		

* - Reported values represent a weighted average of multiple aliquots
† - Erroneous aliquot measurements excluded from reported results

Table 3: Data Summary and Results. All reported errors represent 1σ standard deviations. Production rates and associated corrections (thickness, topographic shielding) are described in Table 2. We deduced the ^{21}Ne – Corrected values from the ^{21}Ne – Initial values following the nucleogenic correction scheme outlined in the Results section of this paper.

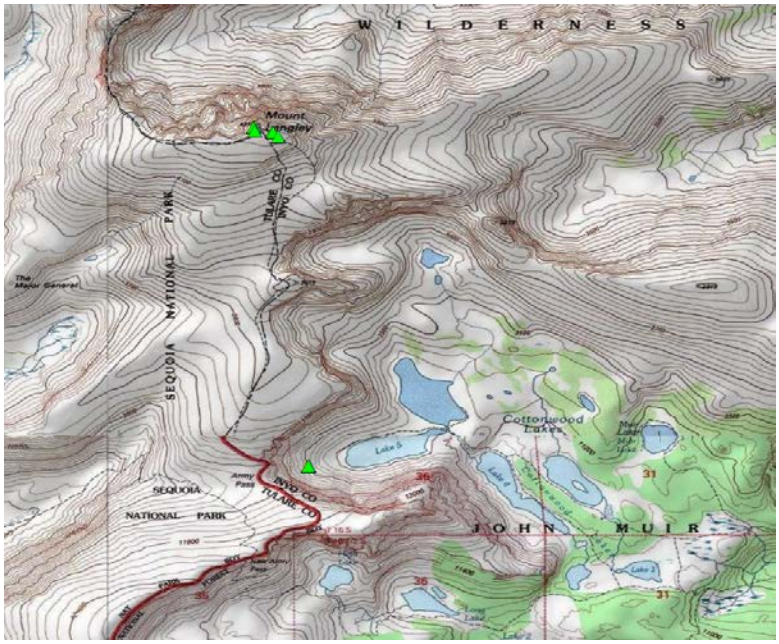

Figure 1: Sample collection sites (green triangles) displayed on United States Topographic Basemap series for Esri ArcMap 10. Data points collected for each sample site using hand-held GPS device. Sample proximity limits individual visibility for summit and cirque floor samples.

Figure 2: Mt. Langley Summit. Note the flat, broad boulders stacked atop one another (regolith mantle), overlying crystalline bedrock. The Mt. Langley summit flat terrain is dominated by boulders similar to those depicted above. Summit boulder samples exhibited highly variable erosion rates among the six summit samples collected.

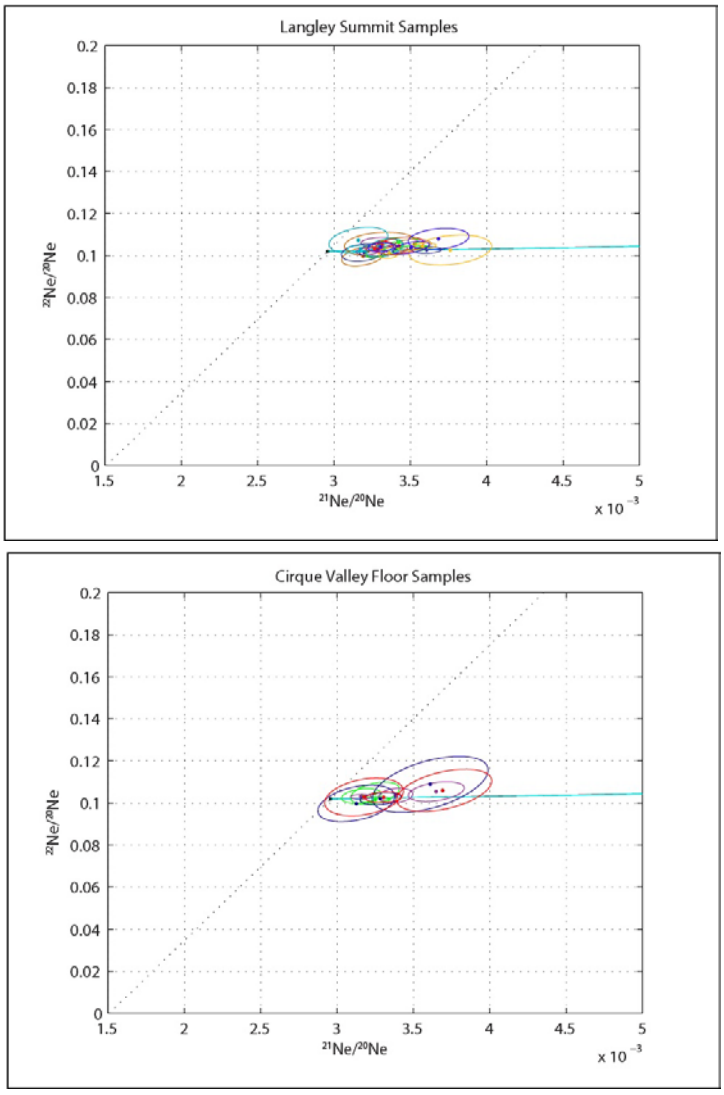

Figure 3: Three isotope plots for summit and cirque floor samples. While the summit sample data points fall along the spallation line, they plot sufficiently low to also seemingly correlate with the nucleogenic composition line. Note that the cirque floor sample points exhibit a poorer fit to the spallation line than the summit sample points.

Appendices

Sample name	wt	^{20}Ne		^{21}Ne		^{22}Ne		21/20		22/20		^{21}Ne cosmogenic via 20		^{21}Ne cosmogenic via 21		Total cosmogenic Ne-21			
	(g)	(Gatoms)	±	(Matoms)	±	(Matoms)	±	(x 1e-3)	±	(x 1e-3)	±	(Matoms/g)	±	(Matoms/g)	±	(Matoms/g)	±	(Matoms/g)	±
Collection Phase 1																			
L1-SUMa-400	0.142	1.65	0.04	5.22	0.17	163.61	4.79	3.19	0.10	99.60	3.20	2.70	1.13	2.35	1.43	16.2	2.37	15.04	3.05
L1-SUMa-800	0.142	2.81	0.04	9.79	0.31	294.29	5.89	3.52	0.09	105.40	1.70	11.06	1.71	10.45	2.36				
L1-SUMa-1100	0.142	1.00	0.02	3.29	0.17	105.30	3.83	3.30	0.17	105.30	4.10	2.44	1.19	2.25	1.30				
L2-SUMa-400	0.151	2.60	0.05	8.46	0.26	265.26	6.12	3.29	0.09	102.80	2.40	5.68	1.49	5.14	2.00	24.33	2.5	22.77	3.63
L2-SUMa-800	0.151	3.83	0.05	13.68	0.39	390.11	6.54	3.61	0.07	102.60	1.10	16.47	1.77	15.68	2.78				
L2-SUMa-1100	0.151	1.44	0.03	4.55	0.16	145.16	4.12	3.19	0.10	101.40	2.90	2.18	0.94	1.94	1.19				
L3-SUMa-400	0.128	2.20	0.05	7.27	0.21	226.81	6.22	3.33	0.09	103.60	3.00	6.38	1.47	5.84	1.97	15.34	2.79	13.67	4.11
L3-SUMa-800	0.128	4.39	0.06	13.79	0.39	450.49	7.64	3.17	0.06	103.30	1.10	7.28	2.08	6.35	3.37				
L3-SUMa-1100	0.128	1.08	0.03	3.39	0.14	115.36	4.04	3.16	0.13	107.30	4.30	1.69	1.13	1.48	1.30				
CVF1a-400	0.153	0.91	0.03	2.88	0.15	93.44	4.94	3.18	0.18	102.80	6.20	1.30	1.08	1.13	1.15	8.81	1.77	7.04	1.7
CVF1a-800	0.153	1.88	0.03	6.17	0.20	192.07	3.96	3.31	0.09	102.70	1.80	4.28	1.05	3.94	1.43				
CVF1a-1100	0.153	0.66	0.03	2.43	0.11	69.87	3.60	3.70	0.21	106.00	6.80	3.23	0.93	3.10	0.92				
CVF2a-400	0.13	1.07	0.04	3.33	0.16	106.38	5.35	3.13	0.17	99.70	6.00	1.38	1.43	1.15	1.53	7.41	1.73	6.88	2.02
CVF2a-800	0.13	1.87	0.03	6.08	0.20	189.45	4.02	3.28	0.09	102.10	2.00	4.68	1.36	4.29	1.75				
CVF2a-1100	0.13	0.54	0.03	1.95	0.10	58.91	3.72	3.61	0.25	108.90	8.90	2.73	1.07	2.59	1.01				
Collection Phase 2																			
L1-SUMb-400	0.272	5.54	0.07	17.47	0.43	557.48	8.81	3.22	0.06	102.00	1.20	5.36	1.13	3.92	1.78	17.23	1.74	13.8	2.54
L1-SUMb-850	0.272	5.48	0.07	18.27	0.38	555.71	9.12	3.40	0.06	103.00	1.10	9.01	1.11	7.57	1.60				
L1-SUMb-1100	0.272	2.31	0.03	7.45	0.22	240.87	4.24	3.30	0.09	106.30	1.60	2.87	0.72	2.31	0.86				
L2-SUMb-400	0.269	6.97	0.16	22.67	0.51	705.74	12.67	3.33	0.08	102.80	2.40	9.58	2.06	7.62	2.57	29.74	2.48	25.21	3.33
L2-SUMb-850	0.269	6.86	0.08	23.96	0.43	698.27	10.82	3.57	0.04	103.50	0.80	15.58	1.05	13.67	1.85				
L2-SUMb-1100	0.269	2.65	0.04	8.88	0.25	276.25	4.83	3.42	0.09	106.20	1.70	4.58	0.89	3.92	1.04				
L4-SUMa-400	0.302	6.33	0.07	20.49	0.46	653.41	10.67	3.32	0.05	104.90	1.20	7.52	1.01	5.91	1.71	17.78	1.57	14.07	2.55
L4-SUMa-850	0.302	7.69	0.09	24.56	0.47	778.59	11.50	3.26	0.04	103.00	0.60	7.80	1.05	6.05	1.79				
L4-SUMa-1100	0.302	1.58	0.03	5.32	0.17	162.91	3.83	3.43	0.11	104.60	2.80	2.46	0.59	2.11	0.64				
L5-SUMa-400	0.31	4.49	0.06	14.86	0.29	448.73	9.24	3.36	0.05	101.30	1.80	5.86	0.75	5.04	1.11	17.55	1.32	15.39	1.78
L5-SUMa-850	0.31	4.72	0.07	16.56	0.35	484.39	7.33	3.58	0.06	104.30	1.10	9.50	0.95	8.36	1.29				
L5-SUMa-1100	0.31	0.84	0.02	3.10	0.14	84.85	3.69	3.76	0.19	102.60	5.00	2.19	0.52	1.99	0.52				
L6-SUMa-400	0.311	5.28	0.07	17.18	0.38	541.17	9.64	3.31	0.06	103.90	1.50	5.91	1.03	4.97	1.40	18.08	1.83	15.62	2.25
L6-SUMa-850	0.311	5.48	0.10	18.79	0.43	557.76	9.33	3.50	0.08	103.70	2.00	9.63	1.43	8.36	1.69				
L6-SUMa-1100	0.311	1.08	0.02	3.92	0.15	114.86	3.45	3.68	0.14	107.90	3.50	2.54	0.49	2.30	0.51				
CVF1b-400	0.303	2.18	0.05	6.97	0.21	224.87	6.51	3.25	0.11	104.60	3.50	2.09	0.79	1.70	0.86	7.22	1.36	5.59	1.63
CVF1b-850	0.303	4.18	0.05	13.30	0.35	416.70	6.29	3.25	0.07	101.50	1.10	4.00	0.98	3.10	1.25				
CVF1b-1100	0.303	1.69	0.03	5.24	0.15	171.58	3.83	3.16	0.09	103.30	2.40	1.12	0.51	0.80	0.59				
CVF2b-400	0.315	3.10	0.05	10.27	0.26	315.67	7.94	3.38	0.08	103.50	2.40	4.20	0.78	3.51	0.95	10.33	1.29	8.22	1.75
CVF2b-850	0.315	5.92	0.07	18.30	0.39	598.47	8.19	3.16	0.05	103.00	0.80	3.72	0.93	2.53	1.40				
CVF2b-1100	0.315	1.09	0.02	3.91	0.13	112.99	2.93	3.65	0.13	105.40	3.20	2.40	0.44	2.18	0.46				

Appendix I: Stepwise Heating and Gas Extraction Data Table. We collected data in two phases. Prior to the first collection phase, sample Ne concentrations were highly uncertain. We used a 400ºC - 800ºC - 1100ºC stepwise heating process in the gas extraction for the first collection phase, and used sample masses ranging from .128g - .153g. Based on the concentrations obtained from Collection Phase 1, we roughly doubled the sample masses for each sample, and used a 400ºC - 850ºC - 1100ºC heating process in gas extraction for Collection Phase 2. The increase in temperature in the second heating stage was implemented in order to ensure full Ne gas extraction. We decided the change in the heating process was necessary due to the relatively large size of the quartz grains collected from the crushed rock mass. Values highlighted in green represent ^{21}Ne concentrations calculated from degassing data which contributed to exposure age and erosion rate calculations. We selected these values because of the smaller calculated error associated with these measurements relative to alternative values produced in data collection.